Nanoscale

ARTICLE

Chirality specific and spatially uniform synthesis of single-walled carbon nanotubes from sputtered Co-W bimetallic catalyst

Received 00th January 20xx,
Accepted 00th January 20xx

DOI: 10.1039/x0xx00000x

www.rsc.org/

Hua An,[a] Akihito Kumamoto,[b] Hiroki Takezaki,[a] Shinnosuke Ohyama,[a] Yang Qian,[a] Taiki Inoue,[a] Yuichi Ikuhara,[b] Shohei Chiashi,[a] Rong Xiang,*[a] and Shigeo Maruyama*[a,c]

Synthesis of single walled carbon nanotubes (SWNTs) with well-defined atom arrangements is widely recognized in the past decades as the largest challenge in SWNTs community, and has become the bottleneck for the application of SWNTs in nano-electronics. Here, we report a selective synthesis of (12, 6) with enrichment of 50%-70% by chemical vapor deposition (CVD) using sputtered Co-W as catalyst. This is achieved in a much milder reduction and reaction condition than the previous report using metalorganic molecule clusters as catalyst precursors (*Nature* **2014**, *510*, 522). Meanwhile, in-plane transmission electron microscope technique unambiguously identified an intermediate structure of Co_6W_6C, which is strongly associated with the selective growth. However, most of W atoms disappear after a 5 min CVD growth, which implies that anchoring W may be important in this mysterious Co-W system.

Introduction

Single walled carbon nanotubes (SWNTs) have attracted much attention during last decades due to the unique structure and thereby interesting electronic properties, including ultra-high carrier mobility and chirality dependent electron conductivity.[1, 2] Various proof-of-concept applications have been demonstrated using this unique electronic properties of this material.[3-5] Though tremendous progresses have been made towards the realistic applications of SWNTs, it is still widely recognized now that the absence of techniques to control the structure/chirality of produced SWNTs has been the bottleneck for the further developments, particularly for those applications in electronics and optics.

Chemical vapor deposition (CVD) has been proposed to be one of the most promising methods to synthesize SWNTs at high efficiencies. However, the produced SWNTs, in almost all cases, contain both semi-conducting and metallic SWNTs with mixed chiralities. Researchers have made significant efforts to explore possible approaches towards structure selective growth from both experimental and theoretical aspects. For example, D. E. Resasco et al. reported a supported CoMo catalyzed synthesis of (6, 5) dominant SWNTs by tailoring the growth conditions and supported materials [6]. Y. Miyauchi et al. resulted a similar chirality enrichment in low temperature alcohol catalytic CVD [7]. J. Liu et al. claimed the synthesis of semi-conducting SWNTs by using ethanol/methanol mixture or by water etching[8-10]. J. Zhang et al. found metallic SWNTs can be destroyed by UV light during growth [11]. A. R. Harutyunyan et al. reported the direct synthesis of metallic SWNTs as high as 91% by modulating the gas ambient during annealing [12]. Y. Chen et al. achieved selective synthesis of (9, 8) with 33.5% abundance among all species [13-15]. B. Yakobson et al. demonstrated that the near armchair SWNTs are kinetically favorable during growth, which results in a greater length and abundance [16]. This model is later supported by B. Maruyama et al. through an *in situ* Raman experiment [17]. More recently, they concurrently considered kinetic and thermodynamic aspects of CNT growth and explains the different enrichments at different CVD conditions.[18]

In spite of these progresses, direct CVD synthesis of single chirality SWNTs has been believed to be challenging. One breakthrough was reported in 2014 by F. Yang, et al., who claimed the selective synthesis of (12, 6) SWNTs at an enrichment of 92% [19]. The key to this high selectivity is the use of Co-W catalyst, which forms Co_7W_6 alloy that has structurally matched (12, 6) SWNTs. The catalyst they used is a unique crown-type structure molecule that contains six Co atoms encapsulated by a W-based polyoxoanion shell, which favors the formation of Co_7W_6 alloy at high temperature [20]. If this growth selectivity is governed by catalyst structure [21] regardless of the precursor molecules, preparing catalyst by more versatile optional methods will not only verify the robustness of this Co-W combination, and may also benefit possible scalable production in the future. In this context, we present here that, by a simple sputtered Co-W catalyst, selective growth can also be achieved with a (12, 6) enrichment of over 70%. An

[a] *Department of Mechanical Engineering, The University of Tokyo, Tokyo 113-8656, Japan.*
E-mail:; maruyama@photon.t.u-tokyo.ac.jp; xiangrong@photon.t.u-tokyo.ac.jp
[b] *Institute of Engineering Innovation, The University of Tokyo, Tokyo 113-8656, Japan*
[c] *Energy NanoEngineering Laboratory, National Institute of Advanced Industrial Science and Technology (AIST), Tsukuba 305-8564, Japan*

Electronic Supplementary Information (ESI) available: Raman spectroscopy (G-band) of SWNTs grown from Co and Co-W catalyst; Kataura plot for chirality assignment; Raman spectra (RBM region) of SWNTs grown from low temperature reduced monometallic Co; Relative intensities of the 197 cm-1 peak with respect to the total sum intensity; TEM image of Co-W catalyst reduced at six different temperatures (600, 650, 700, 750, 800, and 850°C); TEM images of SWNTs grown from Co monometallic catalyst. See DOI: 10.1039/x0xx00000x

intermediate structure of Co_6W_6C is also identified by our recently proposed in-plane transmission electron microscope (TEM) technique, and found to be strongly associated with the selective nucleation.

Results and discussion

Figure 1a shows a representative SEM image of the as-grown SWNTs formed at a growth temperature of 750ºC. A sample grown from pure Co at the same condition is shown as the inset for comparison. Without the existence of W, SWNTs form into a thick mat with a high nucleation density, while in case of Co-W, SWNT density decreases significantly. The length of SWNTs obtained from Co-W after a 5 min growth is usually several micrometers according to higher resolution SEM and TEM observations, which shows no much difference from those obtained from pure Co. The SWNTs grown from Co-W seem to be covered with some amorphous as well as particle-like impurities. This will be further characterized and discussed later. However, since the catalyst is prepared by sputtering, in either case, SWNTs grow uniformly over the entire substrate. This spatial uniformity will be important for future device fabrications.

Raman spectroscopy is used to confirm the existence and the structure of SWNTs. The G-band of both samples (grown from Co and Co-W catalyst) shows typical features of SWNTs, with a clear split into G^+ and G^-. D band of both samples are not strong, and typical G/D ratios are about 15 to 20 (Figure S1). However, clear differences are observed between two samples in Radial Breathing Mode (RBM) regions (Figure 1b). In the case of pure Co, RBM peaks from four laser excitations demonstrate a wide distribution, while for Co-W, though SWNTs with other chiralities also exist, the peak locating at 197 cm^{-1} excited by 633 nm laser becomes dominant. The index of the dominant SWNTs is assigned to be (12, 6) according to the diameter and the excited transition energy in the Kataura plot (Figure S2). The inverse relationship of the RBM frequency and the diameter of the SWNTs is determined by $\omega_{RBM} = 235.9/d_t+5.5$,[22] which was carefully calibrated and specified for SWNTs on flat Si/SiO_2 in this range. (9, 9) is excluded because of the G-band shape which shows an asymmetric G^- with a Breit-Wigner–Fano (BWF) feature.

A Raman mapping was performed to obtain more quantitative results about the SWNT content. In this Raman scanning, a step of 8 μm is used. Since the spot size of laser is smaller than 2 μm and the SWNT length is approximately 2-5 μm from SEM characterization, 8 μm spacing is reasonable to measure one SWNT only once (though in each spot there might exist more than one SWNT), and to avoid the over-count of the same SWNT. By this approach, we measured a 1 cm×1 cm area by four different excitations (totally 1826 points), and obtained 1157 observable RBM peaks, within which 607 are assigned to be (12, 6). From this statistics, if assuming each (12, 6) peak comes from one SWNT, the proportion of (12, 6) peaks among all detectable RBMs can be calculated to about 53%. Considering that there are high possibilities that one peak at 197 cm^{-1} comes from two or more (12, 6) tubes under one laser spot, the real enrichment of (12,6) tubes can be higher. In the original report, F. Yang et al. [19], observed approx. seven SWNTs under one laser spot and concluded a selectivity of over 90%. If assuming there are *x* SWNTs in average under one laser spot, the enrichment in this sample can be calibrated to be 67%, 75%, 82%, 89% if *x* equals to 2, 3, 4, 7, respectively. In our case, the SWNTs are sparser and there are usually 3 to 4 SWNTs in average under one laser post, so (12,6) enrichment after this calibration is over 70% with conservative estimation. We claim this number does not always reflect the exact percentage in SWNTs, because there could be other SWNTs that are not resonant at all these four excitation wavelengths (due to the well-known resonance effect), and/or some SWNTs could be too short to be identified from the background. However, it seems to be clear that the produced SWNT sample is highly (12, 6) enriched according to this Raman analysis, and we conclude here the enrichment is 50-70% from current Raman analysis.

Optical absorption usually gives more reliable evaluations of the entire sample. Figure 1d shows a dominant absorption peak at ~600 nm, which is consistent with M_{11} transition of (12, 6) SWNTs. However, due to the low SWNT yield, the peak is not satisfactorily strong, though over 30 samples were used to prepare one solution. Also, the broad peak suggests the possible coexistence of impurities and other SWNTs. Possibly because of these two reasons, we cannot observe a peak splitting that was clearly shown for spectroscopically pure semimetal SWNTs.[23, 24] Compared with the original report of over 90%,[19] this relatively lower selectivity could be related to the lower growth temperature and/or different catalyst preparation method. Except for this, it is convincing to us that the incorporation of W into Co catalyst leads to a clear shift and narrow down of chirality distribution.

Reduction temperature of catalyst is found crucial for SWNT yield as well as the selectivity of (12,6) SWNTs. Figure 2 shows SEM images and the corresponding average Raman spectra of SWNTs grown from catalyst reduced at different temperatures. In all three cases, the growth temperature was set to the same (750ºC) to compare the possible structure change of catalyst during reduction. When reduction temperature is low (600^o C), the SWNT yield is much higher than the other two samples. The Raman spectrum suggests this low temperature reduced sample is very similar to those grown from pure Co (Fig. S3). The relative intensity of 197 cm^{-1} peak (to other peaks) is remarkably decreased. For samples grown from higher temperature (750^o C) reduced catalyst, however, the (12, 6) peak significantly dominates the RBM peaks (SWNT yield decreased to 5% roughly estimated from Raman). When the reduction temperature goes up to 850^o C, the selectivity slightly improves but the yield becomes much lower. The changes of relative intensities at the 197 cm^{-1} peak with respect to the total sum intensity is shown in Fig. S4, revealing a developing selectivity with the increasing reduction temperature. This trend suggests that even reduction at this relatively low temperature, the introduction of W is still effective for the selectivity, which indicates that the catalyst structure may have already changed. Compared to original

reports by F. Yang et al,[19] where they claimed 1030ºC is necessary, this nearly 300ºC lower reduction/growth temperature is puzzling. If not explainable by somehow further downshift of bulk phase diagram and therefore the easier formation of alloy at lower temperatures, there might be some other un-identified factor that is playing a critical role.

In order to tackle this puzzle, we further performed an in-plane TEM study on these sputtered Co-W catalyst. In these experiments, Co-W catalyst are directly prepared onto a SiO_2 TEM grid. The advantage of this technique is this TEM grid can be used for high temperature reaction.[25] Though the atomic resolution is not always easy due to the thick SiO_2 background, the most original and realistic catalyst morphology and structure are retained. Furthermore, in-plane view also provides a chance to access the statistical information of one sample, which is hardly obtainable in conventional TEM observations.

Figure 3 shows representative TEM images of samples grown at 750 ^{o} C but reduced at different temperatures (similar to samples in Figure 2). In Figure 3a and b, clear differences in the catalyst morphology are observed between two samples. At low reduction temperature (600^{o} C), W and/or C atoms migrate and form a wormlike/island structure, which may be a transition morphology from an as-deposited continuous film (not shown) to nano-sized particles. The 750ºC reduced catalyst (Figure 3b), however, shows more complex and polycrystal-like contrast. Though the melting temperature of W is 3422ºC in bulk, it is apparent that W starts to aggregate and form irregular particles from a temperature as low as 750ºC. Particularly, the regions near larger W particles seem to have been “swallowed” by the center. Therefore, possibly from this stage, W begins to form alloy/composite with Co, and those particles with complex contrast contain both Co and W (structure to be determined later). The 850ºC reduced catalysts in figure 3c show a particle-like morphology similar to 750ºC reduced sample, except that the particles are more spherical and number density is slightly smaller. The simplified illustrations of this change are shown as insets of Figure 3a, b and c. The in-plane images of these samples after SWNT growth are shown in Figure 3d, e, f. The most noticeable difference is the SWNT yield, which agrees well with the SEM and Raman observation (Figure 2). At the same time, all three samples contain particles with diameter 5-30 nm, which are possibly those impurities in SEM observations discussed previously. Besides these three representative samples, we also grew SWNTs from 650ºC, 700ºC and 800ºC reduced catalyst, which show intermediate morphologies (Figure S5). Three reduction temperatures are shown here to demonstrate the clearer trend from islands to spherical particles. In all these observations, identifying the contrast of SWNTs are very difficult due to the strong background of SiO_2. Few layer graphite sheets are sometimes observed on large particles (possibly excess of W as to be discussed later), but no few- or multi-walled carbon nanotubes exist.

One uniqueness of in-plane TEM is its capability of providing comprehensive structural information in a large area. We compared the selected area electron diffraction (SAED) patterns of the samples before and after growth, as shown in Figure 4. In this experiment, each diffraction pattern was taken with the selected area aperture diameter of several micrometers, and therefore contains the average information of more than 10,000 particles. Lower-temperature reduced samples show clear and dominant phase of BCC structure of metallic W (JCPDS-International Centre for Diffraction Data 2004, card no. PDF#04-0806). Co is not visible possibly due to the lower relative amount, alloying with W and/or oxidation after exposure to air. However, since obtained SWNTs are very similar to those from pure Co, probably the interaction between Co and W at this lower temperature is less significant and most SWNTs are grown from pure Co. For high temperature reduced catalyst, additional diffraction rings appear around 110 of metallic W (Figure 4a), suggesting the formation of new crystal phase. These diffraction rings match perfectly with Co_6W_6C (card no. PDF#23-0939). Though the as-reduced catalyst is not supposed to have carbon, this structure is consistently identified in all our experiments where selective growth are achieved. This un-intentionally incorporated carbon (possibly from carbon contamination and/or residue in CVD apparatus) may contribute to the change of catalyst structure from Co_7W_6 to Co_6W_6C. This influence of un-intentionally introduced species is not unique and also reported previously in Fe-based system.[26] Since no additional Co related diffraction patterns are observed, it is very likely this structure is responsible for the nucleation of SWNTs. At this stage we are not able to rule out the possibility of coexistence of some small amounts of metallic Co particles. However, according to the control experiment described previously, pure Co tends to grow SWNTs with wide chirality distribution and thus is unlikely dominant in this case (Fig. S6). Except this ternary Co_6W_6C, no other Co-W alloy phases e.g., Co_7W_6, are identified in all our experiments.

One other interesting phenomenon we found here is that after growth, in both low and high temperature reduced samples, W related phases disappears almost completely. Neither noticeable metallic W nor any other W related phases remain after a 5 min growth. Only existence of pure metallic Co was confirmed by the SAED patterns in Figure 4b. The loss of W species is likely due to a reaction with ethanol during SWNT growth. Ethanol molecules partially decompose at the CVD temperature with water and ethylene as main products.[27] At the same time, metallic W is reported to be easily oxidized in a water vapor environment to form the volatile $WO_2(OH)_2$, which can easily disappear at high temperatures through gas phase [28]. This dynamic change of catalyst structure makes it more challenging to identify the active nucleation sites for growth and suggests that growth time is another important parameter towards more precise control over the selective growth. Further studies may be focused on CVD time dependent (12,6) enrichment. Meanwhile, the yield in the present study is extremely low and we are not yet able to increase carbon yield without compensation of selectivity. Also, it is still unclear whether high selectivity and low yield is always strongly coupled (e.g. an earlier work showed no chirality selectivity for Co-W at a higher carbon yield [29]). Besides growth, more sophisticated

characterizations may be needed for a more precise quantification (e.g. a laser close to 633 nm may excite more SWNT "impurities" that has diameter close to 1.2 nm but were not resonant in current measurement). Nevertheless, we believe that the capability of Co-W bimetallic catalyst in selective growth is well reproduced and the critical role of W in changing the catalyst structure has been clearly demonstrated. Importantly in this work, catalyst is prepared by simple sputtering, which is preferable for future larger scale, more uniform synthesis of SWNTs, and hopefully potential applications using chirality specific SWNT samples. This study also brings out more open questions for this complicated system, which definitely need more efforts from the whole community.

Conclusions

In summary, we demonstrated Co-W catalyst prepared by simple sputtering is capable of producing (12, 6) SWNTs with a selectivity of 50-70% in a much milder growth conditions. Reduction of catalyst is crucial for the selective growth, which only occurs when reduction temperature is above 750ºC. In-plane TEM revealed clear morphology differences between low-temperature and high-temperature reduced catalyst. An intermediate structure of Co_6W_6C is unambiguously identified and associated with the selective growth of (12,6) SWNTs. However, W related structure is also found surprisingly unstable in growth atmosphere after only a few minute growth, suggesting that more efforts are needed for more precise control of this complex Co-W catalyst.

Experimental Methods

Catalyst preparation.

Co-W catalyst is prepared by magnetron sputtering (Ulvac-Riko). The p-doped Si substrate with a 300-nm layer of SiO_2 is attached to the substrate holder and metallic W (nominal thickness 0.7 nm) and metallic Co (nominal thickness 0.3 nm) is deposited in sequence followed by a 5 min annealing at 400 ºC in air. The prepared substrate is used for CVD growth.

SWNT growth.

SWNTs are synthesized by alcohol catalytic chemical vapor deposition (ACCVD).[30] Briefly, the prepared substrate is placed in a 1 inch quartz tube. A 300 sccm Ar/H_2 (3%) mixture gas is purged through the tube during the heating process at a pressure of 40 kPa. Upon reaching the reduction temperature, the sample is kept for another 5 min before heating or cooling to 750^o C in Ar atmosphere (SWNTs are grown at 750^o C in all cases). After that, ethanol is introduced at a flow rate of 150-450 sccm for a 5 min growth at the total pressure of 1.3 kPa. Finally, the tube is cooled down to room temperature with 300 sccm Ar.

SWNT characterization.

As-grown SWNTs are characterized by scanning electron microscope (SEM, Hitachi S-4800) at an accelerating voltage of 1 kV. Raman spectra are obtained by Renishaw inVia, with excitation wavelengths of 488, 532, 633, and 785 nm. Optical absorptions are obtained on the dispersed samples by a UV-vis-NIR optical spectrometer (Shimadzu UV-3150). Since the SWNT yield on surface is not high enough, 20 pieces of 1 cm x 1 cm samples are sonicated in D_2O solution with 1.25 w/v% SDS to obtain enough optical density.

In-plane TEM.

For in-plane TEM characterizations, Co-W catalyst is directly sputtered onto a Si/SiO_2 TEM grid with a SiO_2 (20 nm) fabricated by standard photolithography and etching. The prepared SiO_2 grid is then used for the growth of SWNTs together with standard Si/SiO_2 wafer substrate. TEM images are obtained by JEOL JEM-2000EX-II (JEOL Co. Ltd) and JEM-2010F (JEOL Co., Ltd) operated at 200 keV, and selected area electron diffraction (SAED) patterns are obtained by JEM-2010F with a camera length of 60 cm.

Acknowledgements

We thank T. Ito, H. Tsunakawa for TEM assistance. H.A. thanks the China Scholarship Council for financial support. Part of this work is financially supported by JSPS KAKENHI Grant-in-Aid for Scientific Research (25630063, 15H05760, 26420135), Grant-in-Aid for Young Scientists (15K17984) and JST-EC DG RTD Coordinated Research Project 'IRENA' under the Strategic International Collaborative Research Program (JST-SICORP), and by "Nanotechnology Platform" (project No. 12024046) of the Ministry of Education, Culture, Sports, Science and Technology (MEXT), Japan.

Notes and references

1. R. Saito, G. Dresselhaus and M. S. Dresselhaus, *Physical properties of Carbon Nanotubes*, Imperial Collage Press, 2007.
2. J. Ado, G. Dresselhaus and M. S. Dresselhaus, *Carbon Nanotubes - Advanced Topics in the Synthesis, Structure, Properties and Applications*, Springer, 2008.
3. S. J. Kang, C. Kocabas, T. Ozel, M. Shim, N. Pimparkar, M. A. Alam, S. V. Rotkin and J. A. Rogers, *Nat Nanotechnol.*, 2007, **2**, 230-236.
4. M. M. Shulaker, G. Hills, N. Patil, H. Wei, H. Y. Chen, H. S. PhilipWong and S. Mitra, *Nature*, 2013, **501**, 526-530.
5. A. Javey, J. Guo, Q. Wang, M. Lundstrom and H. J. Dai, *Nature*, 2003, **424**, 654-657.
6. G. Lolli, L. A. Zhang, L. Balzano, N. Sakulchaicharoen, Y. Q. Tan and D. E. Resasco, *J. Phys. Chem. B*, 2006, **110**, 2108-2115.
7. Y. H. Miyauchi, S. H. Chiashi, Y. Murakami, Y. Hayashida and S. Maruyama, *Chem. Phys. Lett.*, 2004, **387**, 198-203.
8. L. Ding, A. Tselev, J. Y. Wang, D. N. Yuan, H. B. Chu, T. P. McNicholas, Y. Li and J. Liu, *Nano Lett.*, 2009, **9**, 800-805.
9. W. W. Zhou, S. T. Zhan, L. Ding and J. Liu, *J. Am. Chem. Soc.*, 2012, **134**, 14019-14026.
10. J. H. Li, C. T. Ke, K. H. Liu, P. Li, S. H. Liang, G. Finkelstein, F. Wang and J. Liu, *ACS Nano*, 2014, **8**, 8564-8572.
11. G. Hong, B. Zhang, B. H. Peng, J. Zhang, W. M. Choi, J. Y. Choi, J. M. Kim and Z. F. Liu, *J. Am. Chem. Soc.*, 2009, **131**, 14642-14643.
12. A. R. Harutyunyan, G. G. Chen, T. M. Paronyan, E. M. Pigos, O. A. Kuznetsov, K. Hewaparakrama, S. M. Kim, D. Zakharov, E. A. Stach and G. U. Sumanasekera, *Science*, 2009, **326**, 116-120.

13. H. Wang, B. Wang, X. Y. Quek, L. Wei, J. W. Zhao, L. J. Li, M. B. Chan-Park, Y. H. Yang and Y. A. Chen, *J. Am. Chem. Soc.*, 2010, **132**, 16747-16749.
14. H. Wang, L. Wei, F. Ren, Q. Wang, L. D. Pfefferle, G. L. Haller and Y. Chen, *ACS Nano*, 2013, **7**, 614-626.
15. L. Wei, B. Liu, X. Wang, H. Gui, Y. Yuan, S. Zhai, A. K. Ng, C. Zhou and Y. Chen, *Adv. Elec. Mater.*, 2015, **1**.
16. F. Ding, A. R. Harutyunyan and B. I. Yakobson, *PNAS*, 2009, **106**, 2506-2509.
17. R. Rao, D. Liptak, T. Cherukuri, B. I. Yakobson and B. Maruyama, *Nature Mater.*, 2012, **11**, 213-216.
18. V. I. Artyukhov, E. S. Penev and B. I. Yakobson, *Nat. Commun.*, 2014, **5**.
19. F. Yang, X. Wang, D. Q. Zhang, J. Yang, D. Luo, Z. W. Xu, J. K. Wei, J. Q. Wang, Z. Xu, F. Peng, X. M. Li, R. M. Li, Y. L. Li, M. H. Li, X. D. Bai, F. Ding and Y. Li, *Nature*, 2014, **510**, 522-524.
20. S. Yao, Z. Zhang, Y. Li and E. Wang, *Dalton Transactions*, 2010, **39**, 3884-3889.
21. F. Yang, X. Wang, D. Q. Zhang, K. Qi, J. Yang, Z. Xu, M. H. Li, X. L. Zhao, X. D. Bai and Y. Li, *J. Am. Chem. Soc.*, 2015, **137**, 8688-8691.
22. D. Zhang, J. Yang, F. Yang, R. Li, M. Li, D. Ji and Y. Li, *Nanoscale*, 2015.
23. X. M. Tu, A. R. H. Walker, C. Y. Khripin and M. Zheng, *J. Am. Chem. Soc.*, 2011, **133**, 12998-13001.
24. E. H. Haroz, J. G. Duque, X. M. Tu, M. Zheng, A. R. H. Walker, R. H. Hauge, S. K. Doorn and J. Kono, *Nanoscale*, 2013, **5**, 1411-1439.
25. K. Cui, A. Kumamoto, R. Xiang, H. An, B. Wang, T. Inoue, S. Chiashi, Y. Ikuhara and S. Maruyama, *Nanoscale*, 2016, **8**, 1608-1617.
26. B. C. Bayer, C. Baehtz, P. R. Kidambi, R. S. Weatherup, C. Mangler, J. Kotakoski, C. J. L. Goddard, S. Caneva, A. Cabrero-Vilatela, J. C. Meyer and S. Hofmann, *Appl Phys Lett*, 2014, **105**, 143111.
27. R. Xiang, B. Hou, E. Einarsson, P. Zhao, S. Harish, K. Morimoto, Y. Miyauchi, S. Chiashi, Z. K. Tang and S. Maruyama, *ACS Nano*, 2013, **7**, 3095-3103.
28. B. Zhou, S. Han, R. Raja and G. A. Somorjai, *Nanotechnology in catalysis 3*, Springer Science & Business Media, 2007.
29. J. E. Herrera and D. E. Resasco, *J. Phys. Chem. B*, 2003, **107**, 3738-3746.
30. S. Maruyama, R. Kojima, Y. Miyauchi, S. Chiashi and M. Kohno, *Chem. Phys. Lett.*, 2002, **360**, 229-234.

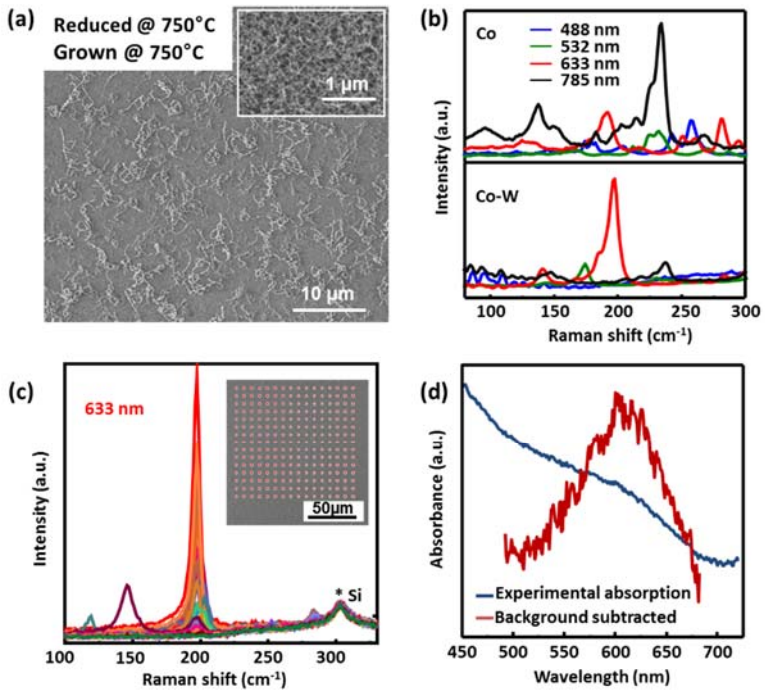

(e)

Excitation laser wavelength (nm)	488	532	633	785	total
Number of RBM peaks	21	161	952	23	1157
Number of (12,6) peaks (~197 cm^{-1})	0	0	607	0	607

Proportion of (12,6) peak among all RBM= 607/1157=53%
Calibrated enrichment of (12,6) among all SWNTs=75%

Figure 1|Characterization of SWNTs grown from sputtered CoW. (**a**) A typical SEM image of SWNTs grown from CoW inset with the SWNTs arrays obtained from pure Co. (**b**) Averaged Raman spectra in RBM region of SWNTs grown from pure Co and CoW with four different excitation wavelengths. (**c**) Raman spectra of SWNTs with multi data excited at 633 nm. (**d**) An optical absorption spectrum of SWNT samples after dispersion. (**e**) Statistical analysis on SWNTs of (12, 6) with RBM occurrence frequencies excited by four lasers: 488, 532, 633 and 785 nm.

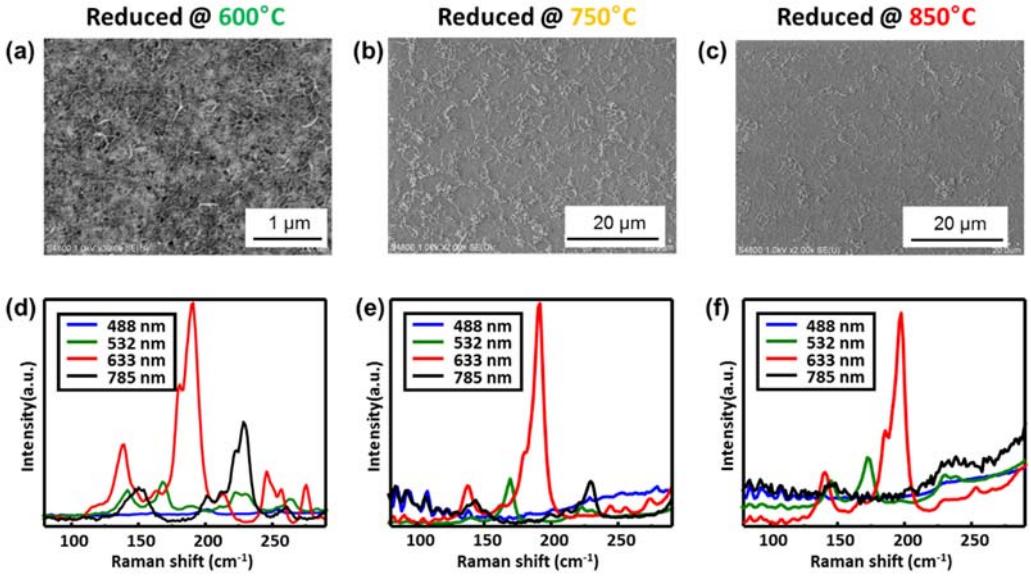

Figure 2| SEM images and average Raman spectra of SWNTs grown at different reduction temperatures: (**a, d**) 600^{o} C, (**b, e**) 750^{o} C and (**c, f**) 850^{o} C.

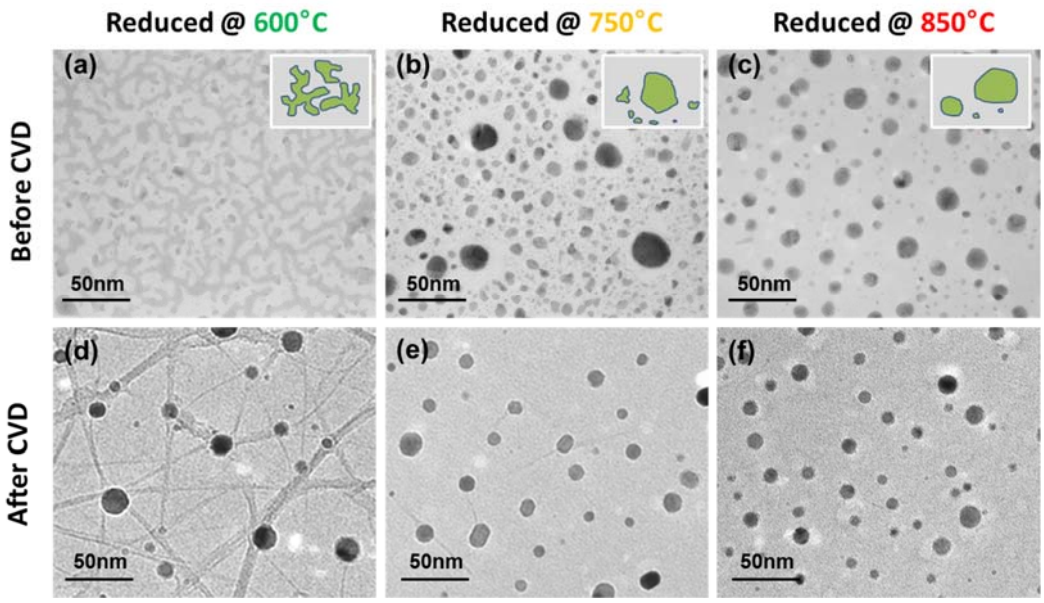

Figure 3| TEM micrographs of different temperature reduced (600°C, 750°C and 850°C, respectively) CoW catalyst. (**a**), (**b**), (**c**) before CVD and (**d**), (**e**), (**f**) after a 5 min growth at 750° C.

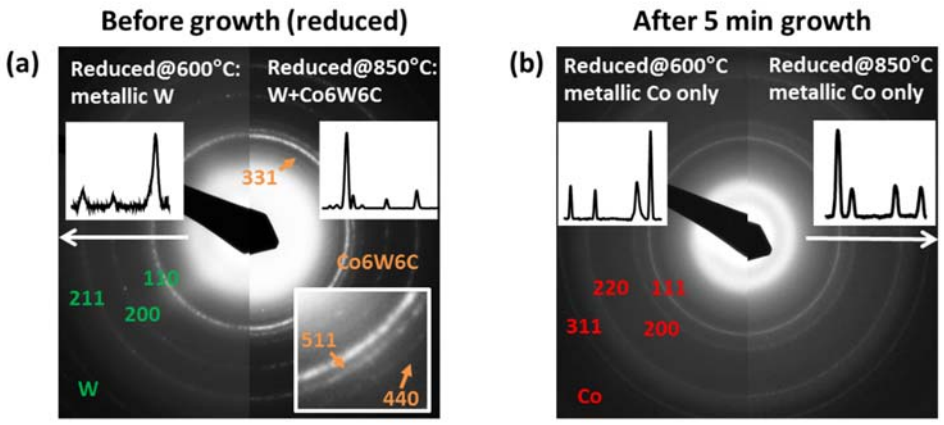

Figure 4| Electron diffraction patterns of catalysts reduced at 600°C, 850°C. (**a**) before and (**b**) after growth with the assigned materials and structure. Inset in (b) is the relative intensity of electron diffraction rings.